

Appendix A

A “flip-flop” rotation stage for routine dual-axis electron cryotomography

Cristina V. Iancu^{†1}, Elizabeth R. Wright^{†1}, Jordan Benjamin¹, William F. Tivol¹,
D. Prabha Dias¹, Gavin E. Murphy¹, Robert C. Morrison², J. Bernard Heymann³, and
Grant J. Jensen^{1*}

¹Division of Biology, California Institute of Technology, 1200 E. California Blvd.,
Pasadena, CA 91125

²Gatan (UK), 25 Nuffield Way, Abingdon Oxon OX14 1RL UK

³Current address: Laboratory of Structural Biology Research, National Institute of
Arthritis, Musculoskeletal and Skin Diseases, National Institutes of Health, Bethesda,
Maryland 20892

[†]These authors contributed equally

*To whom correspondence should be addressed: jensen@caltech.edu, 626-395-8827
(phone) 626-395-5730 (fax)

Published in *Journal of Structural Biology* Volume 151, Issue 3, September 2005, Pages
288–297

doi:10.1016/j.jsb.2005.07.004

Received 3 March 2005; revised 6 June 2005; accepted 6 July 2005. Available online 11
August 2005.

Abstract

Electron cryotomography can be used to solve the three-dimensional structures of individual large macromolecules, assemblies, and even small intact cells to medium (~4–8 nm) resolution in a near-native state, but restrictions in the range of accessible views are a major limitation. Here we report on the design, characterization, and demonstration of a new “flip-flop” rotation stage that allows facile and routine collection of two orthogonal tilt-series of cryosamples. Single- and dual-axis tomograms of a variety of samples are compared to illustrate qualitatively the improvement produced by inclusion of the second tilt-series. Exact quantitative expressions are derived for the volume of the remaining “missing pyramid” in reciprocal space. When orthogonal tilt-series are recorded to $\pm 65^\circ$ in each direction, as this new cryostage permits, only 11% of reciprocal space is left unmeasured. The tomograms suggest that further improvement could be realized, however, through better software to align and merge dual-axis tilt-series of cryosamples.

Keywords:

tomography, electron microscopy, cryoEM, dual-axis, cryoholder, missing wedge

Introduction

The highest resolution technique currently available for three-dimensional structural studies of unique objects is electron tomography, in which a specimen is imaged multiple times in an electron microscope (EM) while being incrementally tilted through a range of views. The method has the potential to couple the exquisite spatial resolution of modern electron microscopes, which in some cases can now be even sub-Angstrom [1, 2], with three-dimensional structure determination through a variety of reconstruction algorithms. Thus electron tomography is emerging as a powerful new technique in both materials and life science research [3-5].

There are several practical limitations for biological samples, however, including radiation damage and the typically restricted range of tilt-angles from which images can be recorded. The tilt-angle limitation arises because most EM samples are thin disks of material approximately 3 mm in diameter and ~ 30–500 nm thick, and as these samples are incrementally tilted, the depth of material the electron beam must pass through increases as one over the cosine of the tilt-angle. At high tilt-angles, most samples become prohibitively thick. In addition, the edges of standard sample holders block the electron beam at high tilt-angles. Because each projection image provides the amplitudes and phases of just one central section of the specimen's three-dimensional Fourier transform, this data collection constraint translates into a "missing wedge" of information in reciprocal space.

Early in the development of electron tomography, this missing wedge problem was significantly reduced for room temperature samples by collecting two tilt-series

about orthogonal axes, thus reducing the missing “wedge” to just a missing “pyramid” [6, 7]. This procedure was relatively straightforward because room-temperature samples could be removed from the microscope and the specimen holder, manually rotated 90°, and replaced for collection of the second tilt-series without much challenge. Despite complications due to the shrinking and warping of plastic-embedded sections during data collection, dramatic improvements in the quality of the tomograms were realized by inclusion of the second tilt-series, and dual-axis tomography became the recognized standard, best practice [8].

Concurrently, various improvements in microscope technology and sample preparation made it possible to image biological materials in a life-like, “frozen-hydrated” state. Such samples are produced by either plunge-freezing thin films [9] or cryosectioning high-pressure-frozen bulk samples [10, 11]. These developments have made it possible to study the three-dimensional structures of unique objects, including even whole cells *in their near-native states* [5], and strong efforts are now being invested to maximize resolution and interpretability.

One of the challenges has been the development of a cryostage that allowed facile collection of two perpendicular tilt-series. Because frozen-hydrated samples must always be kept at very low temperatures (standard practice is to maintain better than -160° C) to prevent ice crystallization, they cannot be simply removed from the microscope, rotated 90° and replaced unless it is done under cold nitrogen gas. This is awkward at best, and is not routinely successful because of the difficulty of fine grid manipulations under these conditions and the frequency of grid contamination. In an attempt to allow grid rotation within the microscope column, the Martinsreid group, in collaboration with Gatan,

modified a standard cryostage and then used it to collect dual-axis tilt-series of at least one frozen-hydrated sample [12], but the stage was not described and seems not to have been used in recent work from the same group [13-16]. A motor-driven tilt-rotation holder (the Gatan CT3500RT) has also been developed for standard side-entry goniometers, but no results of its use in this context are yet available. Here we report on the design, characterization, and experimental benefit of a new “flip-flop” cryorotation stage that allows routine dual-axis cryotomography in the FEI Polara transmission electron microscope, and identify new image processing challenges this type of data presents.

The flip-flop rotation stage

The “flip-flop” rotation stage was an experimental product designed and built by Gatan UK (RCM) in consultation with Caltech (GJJ) and others. The prototype was then tested and characterized experimentally at Caltech, as reported below. The stage is a derivative of the new cartridge-based, multispecimen stage system implemented to accommodate liquid-helium sample-cooling in the new Polara series of TEMs from the FEI Company. Frozen-hydrated grids are first clamped into cartridges, and then up to six cartridges at a time are loaded into a multispecimen holder. The holder is sealed, evacuated, mounted on the microscope column, and then opened to the column vacuum. Individual cartridges are picked up with an insertion tool and introduced into the column proper, where they are threaded onto a permanently-inserted specimen rod.

The flip-flop rotation stage consists of modified cartridges and a special rotation tool in the multispecimen holder. The modified cartridges house an inner, rotationally

mobile cup into which the grid is clamped (Fig. A-1A). This mobile cup has two protrusions extending out beyond the edge of the cartridge in opposite directions. The rotation tool is like a two-car garage, in that it can house cartridges in either side, but unlike a garage, it moves over and around the cartridges while they remain fixed (Fig. A-1B). When a cartridge is docked in the multispecimen holder, the rotation tool can be pushed over the cartridge (Fig. A-1C) in such a way that it catches one of the protrusions on the inner cup and causes the cup to rotate 90°. Depending on which docking position the cartridge occupies in the multispecimen holder, pushing the rotation tool causes the cup to be rotated into either the “flip” position or the “flop” position, 90° away.

Collection of a dual-axis tilt-series proceeds as follows. A cryosample is clamped into the cup of a flip-flop cartridge and loaded into the multispecimen holder. The multispecimen holder is mounted onto the microscope, the flip-flop cartridge is moved to position 5 in the multispecimen holder, and the rotation tool is pushed over the cartridge to ensure the cup begins in the “flip” position. Then the cartridge is introduced into the column, threaded onto the specimen rod, and a suitable specimen is located and imaged through one tilt-series. The cartridge is then retrieved from the column and placed into position 6 of the multispecimen holder, all the while protected by the microscope’s column vacuum. The rotation tool is once again pushed over the cartridge, this time rotating the cup and grid into the “flop” position. The cartridge is again threaded onto the specimen rod, the object of interest is re-located, and the second, orthogonal tilt-series is recorded.

Technical characterization

One of the challenges for any cryostage is to minimize thermal drift. The grid must be in good, uniform, thermal contact with the cryoholder. There was concern that the rotating cup in the flip-flop cartridge would make poor contact with the rest of the cartridge and cause drift. Fortunately, no more drift was observed with the flip-flop cartridges than with regular cartridges, and both are impressively stable. A simple test grid with colloidal gold on carbon was allowed to equilibrate in the column at liquid nitrogen temperature for several hours. The drift rate was then measured at one-minute intervals for five minutes, manifesting displacements of 0.7, 0.8, 0.4, 0.3, and 0.3 nm (average 0.5 nm per minute).

Next, the actual rotation realized and the vertical displacement of the grid effected by the rotation were measured by setting eucentric height, recording a nominally untilted image, rotating the sample with the flip-flop mechanism, refinding the target region, resetting eucentric height, and recording a second nominally untilted image. In nine trials involving three different flip-flop cartridges, the rotation angle ranged from 87.0° to 88.8°, with an average of 87.7° and a standard deviation of 0.6°. The vertical displacements ranged from 0.15 to 2.65 μm , with an average of 1.07 μm and a standard deviation of 0.73 μm .

The dose needed to re-center the target region under the beam after rotation can be reduced to arbitrarily low values, including zero. The grid coordinate system can be re-oriented by imaging markers around the target region, for instance, which allows objects to be re-centered simply by moving to their new coordinates. Fine re-centering can be done by finding “focus” spots close to but on either side of the target. More

routinely, however, we have re-centered targets directly with low dose, low magnification images that deliver less than 1 electron/Å². All other preparative steps can be performed on peripheral areas, including resetting the eucentric height and re-centering the energy filter slit if necessary.

Qualitative comparisons of single- versus dual-axis tomograms

Using the flip-flop stage, dual-axis tomograms of a variety of representative frozen-hydrated specimens were produced including whole bacterial cells, virus-like-particles, bacterial carboxysomes, and solutions of purified proteins. The whole cell chosen was the bacterium *Mesoplasma florum*, a very small and simple cell that inhabits citrus plants. *M. florum* cells were plunge-frozen on Quantifoil grids into liquid ethane using an FEI Vitrobot. A tilt-series was collected from -66° to +62° with a 1° tilt step, and then the grid was rotated ~ 90° about the z-axis and a second tilt-series was collected from -62° to +66°. The total dose used for each tilt-series was 60 e-/Å², the defocus was ~ 15 µm (first CTF zero at ~ 1/5.5 nm), and the magnification was set such that each CCD pixel represented 1.34 nm on the specimen. All images here and below were energy-filtered (slit width of 20 eV) and recorded on a 300 kV FEG “G2 Polara” TEM with the sample cooled by liquid nitrogen to ~ 82 K.

Three-dimensional tomograms of the first and second tilt-series were calculated and combined using the IMOD package [7], and then the individual and combined tomograms were denoised by 40 rounds of nonlinear anisotropic diffusion [17]. Fig. A-2 shows slices through the centers of three tomograms of a *M. florum* cell: one from each of the two independent tilt-series and one from their combination. All the XY slices (left

column) are comparably well-defined, and many individual large protein complexes are resolved within the cell. Nevertheless, while the tomogram from the first tilt-series (top row) shows some detail in the XZ slice (albeit smeared in the Z direction), the YZ slice is quite poor. The tomogram from the second tilt-series (middle row) is the opposite, showing some detail in the YZ but not the XZ slice. Only in the dual-axis tomogram (bottom row) are particles resolved in all three directions. The residual missing pyramid of data is still evident, though, in the membrane's lack of closure over the top and bottom surfaces of the cell.

Next, the impact of including a second tilt-series was observed on a purified, HIV-1 virus-like particle (VLP). HIV-1 is an enveloped retrovirus whose outer layer consists of a lipid bilayer and a matrix protein shell. In these VLPs, the Env protein was removed to eliminate infectivity, so no surface “spikes” are seen. Inside the lipid/matrix layer there is a typically conical capsid shell [18]. An HIV-1 VLP was plunge-frozen, imaged through orthogonal tilt-series, reconstructed, and denoised as described above for *M. florum*, except that the tilt-series were from -57° to $+60^\circ$ and -60° to $+60^\circ$ with a 3° tilt step, the defocus was $\sim 16 \mu\text{m}$ (first CTF zero at $\sim 1/5.6 \text{ nm}$), the image pixel size was 1.34 nm , the total dose was $240 \text{ e}^-/\text{\AA}^2$, and only 20 rounds of denoising were performed (Fig. A-3). Although still not complete, the dual-axis tomogram resolved significantly more of the viral layers' morphologies than either single-axis tomogram. This was made particularly obvious in the three-dimensional renderings of the viral envelope isosurface. The improved but still imperfect point-spread-function was also evidenced by the gold fiducial, which appeared nicely round in the XY plane, but still elongated in the Z direction.

In the two previous cases (MF and HIV-1), comparisons were made between single-axis tomograms and their dual-axis combinations. While this eliminated structural differences between the compared objects, the dual-axis tomograms unfairly profited from twice the dose. Two additional samples were therefore tested where single- and dual-axis tomograms could be calculated from separate but very similar objects, using the same *total* dose. The first such sample was purified carboxysomes from the prokaryote *Synechococcus species*. Carboxysomes are ~ 100 nm microcompartments consisting of a proteinaceous shell surrounding many tens of copies of the enzyme ribulose 1,5-bisphosphate carboxylase/oxygenase (RuBisCO), as well as other, smaller enzymes [19]. Carboxysomes were plunge-frozen and imaged through either a single tilt-series or through two orthogonal tilt-series, in every case to $\pm 64^\circ$. The dose (total) was $120 \text{ e}^-/\text{\AA}^2$, the tilt step was 2° , the defocus was ~ 10 μm (first CTF zero at ~ 1/4.5 nm), the image pixel size was 6.7 \AA , and 200 rounds of denoising were performed. The protein shell and many individual RuBisCO molecules can be resolved in the tomograms (Fig. A-4). Again the resolution of the dual-axis tomogram is clearly more isotropic, but still not as good in the Z direction as in the X or Y directions.

Finally, several different purified protein complexes were imaged, including the molluscan hemocyanin from *Megathura crenulata*. This hemocyanin is an ~ 8 MDa complex that forms a double-layered, hollow barrel approximately 30 nm in diameter and 35 nm in length. Hemocyanin was plunge-frozen and imaged through single- (-66° to 63°) and dual-axis (-66° to 63° first axis, $\pm 63^\circ$ second) tilt-series with an angular step size of 3° , a defocus of 8 μm (first CTF zero at ~ 1/4.0 nm), and a pixel size of 6.7 \AA . Single- and dual-axis tomograms were recorded with the same total dose ($110 \text{ e}^-/\text{\AA}^2$) from

different holes in the same square of a single grid with as similar ice thicknesses and other characteristics as possible. Three-dimensional renderings of particles that froze with their long axes in the plane of the sample and either parallel or perpendicular to the tilt-axis, and with their long axis perpendicular to the sample (“vertical”) are shown (Fig. A-5) after 20 rounds of denoising and alignment to a reference [20] using the BSOFT software package [21]. The particles were not symmetrized before rendering. While the dual-axis tomograms are perhaps just slightly better, the improvement was more modest than expected. As discussed below, this is probably due to non-optimal merging of the two tilt-series, which was most challenging in this case of isolated protein complexes.

Novel data processing challenges

The IMOD software package [7] was used to produce all these tomograms. The procedure begins by calculating two independent, real-space tomograms from the two tilt-series, and then the second tomogram is transformed into approximate alignment with the first using the coordinates of corresponding gold fiducials. The second tomogram is then sampled with an array of subvolumes (“patches”), and each patch is cross-correlated with a corresponding patch from the first. A map of the resulting displacement vectors is fit to a smooth function, and a new, “dewarped” version of the second tomogram is calculated. The dewarped second and the first tomograms are Fourier transformed and averaged in reciprocal space, and then a final, dual-axis tomogram is produced by inverse transformation. While these algorithms have been used and refined extensively to merge tilt-series of plastic sections, the data from cryosamples can be different in important ways: (1) the gold beads are typically distributed throughout the sample rather than just

on the top and bottom surfaces; (2) no shrinkage or distortion during data collection is expected; (3) images are more noisy due to the stringent dose limitations; and (4) contrasty objects can be more sparse, as, for instance, the isolated hemocyanin molecules were against the feature-less background of vitreous ice.

These differences introduced novel image processing problems. First, while no evidence for shrinking or warping was seen, a small fraction of the gold fiducials used to align the two tilt-series moved by up to several nm during acquisition of the data. Because no reproducible pattern was recognized, this mismatch is likely caused by the fiducials diffusing randomly within the vitreous ice. Thus their movements were sometimes significant, but not correlated with movements of neighboring objects of interest (unlike fiducials on the surface of a shrinking plastic section).

Next, the strategy of mapping local distortions between the first and second tomograms seemed non-ideal in this context, especially for the isolated protein complexes. In the case of hemocyanin, for instance, the best results were obtained when exceedingly large patches and high “warping residual limits” were used. This is probably because small patches sometimes contained only vitreous ice, and were therefore nearly featureless, and yielded misleading distortion vectors. To solve this problem, IMOD already allows users to identify specific regions to be included in the dewarping procedure, and discard anomalous vectors, but superior results would likely be obtained by using each reconstructed macromolecular complex as a “patch.” An iterative refinement procedure in which all the images from both tilt-series were re-aligned to projections of the reconstructed object of interest (as in standard “single particle analysis,” see [22], might be best of all. In principle, the structure of cryosamples should

not be changing during data collection, and thus no dewarping at all should be necessary. Slight changes in the electron optics, non-idealities of the tilt-axis, and distortions caused by the energy filter are still probably introducing slight distortions which can and should be corrected.

Finally, it was observed that in the three-dimensional power spectra of the final tomograms, the average intensity in regions where data was combined from both tilt-series was lower than the average intensity in regions covered by just one or the other (Fig. A-6a). The algorithm used in IMOD to merge tilt-series was a simple average: In regions of reciprocal space where there was data from both or neither tilt-series, the two values were simply averaged vectorially; whereas in regions where there was data from just one tilt-series, that single value was used. While this seems entirely reasonable, the reduced amplitudes in doubly-measured regions can be explained simply by the fact that the average length of two vectors is always larger than the length of their *vector* average, except in the rare case that their directions (phases) are identical. While this difference may not be large for well-aligned data with a high signal-to-noise ratio, it was apparent in these cryotomograms. D. Mastronarde therefore introduced an IMOD option to simply attenuate the amplitudes in the singly-measured regions to match those in the doubly-measured regions within shells of reciprocal space (Fig. A-6b). Whether this is the optimal procedure has yet to be explored.

Size of the missing pyramid in single- versus dual-axis data collection

The potential benefit of dual-axis tomography can be assessed quantitatively by calculating the percentage of reciprocal space covered by single- and dual-axis tilt-series.

While isolated results of similar calculations already appear in the tomography literature, the formulas and their derivations do not to our knowledge, and because they involve principles of spherical trigonometry unfamiliar to most investigators in this field, they are presented here. In spherical trigonometry, lengths and areas are quantified in degrees and “spherical” degrees, respectively, and by “spherical polygon” is meant a region on the surface of a sphere whose borders are defined by planes passing through the sphere’s origin. The area of a spherical polygon in spherical degrees is equal to its angular excess; i.e., the amount by which the sum of its angles exceeds that of an analogous polygon on a plane. For example, on a globe the spherical triangle formed by a segment of the equator and two meridians of longitude has an area equal to the angle between the meridians, since the angles between each meridian and the equator is 90° , and account by themselves for the sum of the three angles of a planar triangle.

Making the assumption that the flip-flop holder yields two tilt-series that are indeed orthogonal, but allowing different maximum tilt-angles in both the positive and negative direction for both tilt-axes, one can calculate the size of the missing pyramid using Fig. A-7. The view is down the direction of the electron beam, or Z axis, and the four large arcs (two splitting away from and rejoining the X axis and two splitting away from and rejoining the Y axis) represent the limits of the two tilt-series. Thus the first tilt-series (along X) is from α_{\min} to α_{\max} , and the second tilt-series (along Y) is from β_{\min} to β_{\max} . These arcs should be thought of as lying on the surface of a sphere in reciprocal space, while the X and Y axes lie within an “equatorial” plane below, such that they do not intersect with the arcs except at the endpoints. Since the totality of information out to any specified resolution is a sphere, and since the solid angle of the missing pyramid is

the same regardless of the sphere's radius, the fraction of missing information is the ratio of the area of the spherical quadrilateral bounded by the planes of maximum tilts (shaded region) to the area of the full hemisphere, or 360 spherical degrees. The missing area is equal to its angular excess, or $(180^\circ - \theta^{++}) + (180^\circ - \theta^{+-}) + (180^\circ - \theta^{-+}) + (180^\circ - \theta^{--}) - 360^\circ$. Napier's rules for right spherical triangles state that the cosine of one of the non-right angles is equal to the sine of the other non-right angle times the cosine of the opposite side length. Thus $\cos(\theta^{++}) = \sin(90^\circ - \alpha_{\max})\cos(\beta_{\max})$, or $\cos(\alpha_{\max})\cos(\beta_{\max})$. Similarly, $\cos(\theta^{+-}) = \cos(\alpha_{\min})\cos(\beta_{\max})$, $\cos(\theta^{-+}) = \cos(\alpha_{\min})\cos(\beta_{\min})$, and $\cos(\theta^{--}) = \cos(\alpha_{\max})\cos(\beta_{\min})$. Given α_{\min} , α_{\max} , β_{\min} , and β_{\max} , the percentage of missing information can be found by calculating the angles θ , and then the angular excess of the missing region. Note that the formulas are symmetric with respect to which angles are called α and β , which directions are called "max" and "min," and give correct results at limiting values, including the case of single-axis tilting.

Several key results are listed in Table A-1. In order to reduce the missing information to just 10% (an arbitrary example target) with single-axis tilting, $\pm 81^\circ$ must be obtained. This is of course fundamentally problematic, because thin films are 6.4 times thicker parallel to the electron beam at 81° than they are untilted. For dual-axis tilting, reducing the missing pyramid to 10% requires reaching just 67° , where the sample is only 2.6 times thicker. The flip-flop cartridges allow imaging to $\pm 65^\circ$, so that all but 11% of the data can be gathered for a thin sample.

Discussion

From this work we conclude that: (1) the new flip-flop holder succeeds in making the collection of dual-axis tilt-series of cryosamples convenient and routine, (2) including the second tilt-series does result in more isotropic resolution as expected, but (3) further gains should be realizable through better software to merge the data. The flip-flop holder has been used to collect more than a hundred dual-axis tilt-series of various samples now, of which only a few examples were shown here. These demonstrated that inclusion of the second tilt-series clarified the morphology of membranes, protein shells, and individual protein complexes. We have since observed other cases where dual-axis tilting has proven critical—including one dramatic case where a key bacterial cytoskeletal filament was essentially invisible in the tomogram of the first tilt-series, but was clearly resolved in the second. Except for the 90° rotation, the two tilt-series were otherwise identical in defocus, etc., and of course radiation damage does not explain the difference, since the filament was seen in the second tilt-series but not the first. Instead, this filament exemplified how long, tubular features that lie perpendicular to the tilt-axis are nearly invisible to single-axis tomography.

Despite these encouraging improvements, the results also suggest that better methods for alignment and merging are needed. This study is the first attempt to our knowledge to merge dual-axis tilt-series of isolated macromolecules suspended in vitreous ice. Considering the range of views used in the hemocyanin tomograms, the dual-axis tomograms theoretically profited from an additional 15% coverage of reciprocal space (72% for the single-axis tomograms, 87% for the dual). The gains experimentally realized in this particular case (as seen in Fig. A-5) were only modest. We attribute this to

non-optimal alignment and merging, which should be improved by more customized software.

Finally, the cartridge-based specimen holder system was originally designed to allow samples to be cooled with liquid helium rather than liquid nitrogen, in hopes that radiation damage could be further slowed or restrained. One of the potential disadvantages of the flip-flop stage design was that the sample had to be warmed to approximately -190°C between tilt-series for rotation because the multispecimen holder is only nitrogen-cooled. Thus the potential advantages of helium-cooling would be lost mid-way. Disappointingly, this is no longer a concern. Only disadvantages have been observed for liquid helium-cooling in cryotomography, and we now routinely use only liquid nitrogen. As part of the present investigations, however, the effects of warming helium-cooled samples to -190°C for rotation in the multispecimen holder were extensively explored. While the results will be reported in full alongside related experiments evidencing phase transitions in vitreous ice (manuscript in preparation), we note here that the warming associated with rotation did indeed relax some radiation-induced strains. The relaxation was a net advantage, however, if anything, as it tended to restore lost contrast and delay the appearance of small bubbles.

Acknowledgements

We thank D. Mastronarde for assistance with IMOD, H.J. Ding and B. Wen for image processing, A. Martino for providing purified carboxysomes, W. Sundquist for purified HIV-1 virus-like particles, and S. Tivol for reading the manuscript. This work was supported in part by NIH Grant PO1 GM66521 to GJJ, DOE grant DE-FG02-04ER63785

to GJJ, the Beckman Institute at Caltech, and gifts to Caltech from the Ralph M. Parsons Foundation, the Agouron Institute, and the Gordon and Betty Moore Foundation.

References

1. Batson, P.E., N. Dellby, and O.L. Krivanek, *Sub-angstrom resolution using aberration corrected electron optics*. Nature, 2002. **418**(6898): p. 617-20.
2. Hosokawa, F., et al., *A spherical aberration-corrected 200 kV TEM*. J. Electron Microsc., 2003. **52**(1): p. 3-10.
3. Ziese, U., K.P. de Jong, and A.J. Koster, *Electron tomography: a tool for 3D structural probing of heterogeneous catalysts at the nanometer scale*. Applied Catalysis A:General, 2004. **260**(1): p. 71-74.
4. Subramaniam, S. and J.L.S. Milne, *Three-dimensional electron microscopy at molecular resolution*. Annu. Rev. Biophys. Biomol. Struct., 2004. **33**: p. 141-155.
5. Baumeister, W., *Mapping molecular landscapes inside cells*. Biol. Chem., 2004. **385**(10): p. 865-72.
6. Penczek, P., et al., *Double-Tilt Electron Tomography*. Ultramicroscopy, 1995. **60**(3): p. 393-410.
7. Mastrorarde, D.N., *Dual-axis tomography: an approach with alignment methods that preserve resolution*. J. Struct. Biol., 1997. **120**(3): p. 343-52.
8. McEwen, B.F. and M. Marko, *The emergence of electron tomography as an important tool for investigating cellular ultrastructure*. J. Histochem. Cytochem., 2001. **49**(5): p. 553-64.

9. Dubochet, J., et al., *Cryo-electron microscopy of vitrified specimens*. Q. Rev. Biophys., 1988. **21**(2): p. 129-228.
10. Hsieh, C.E., et al., *Electron tomographic analysis of frozen-hydrated tissue sections*. J. Struct. Biol., 2002. **138**(1-2): p. 63-73.
11. Al-Amoudi, A., et al., *Cryo-electron microscopy of vitreous sections*. EMBO J., 2004. **23**(18): p. 3583-8.
12. Nickell, S., et al., *Pyrodictium cannulae enter the periplasmic space but do not enter the cytoplasm, as revealed by cryo-electron tomography*. J. Struct. Biol., 2003. **141**(1): p. 34-42.
13. Beck, M., et al., *Nuclear pore complex structure and dynamics revealed by cryoelectron tomography*. Science, 2004. **306**(5700): p. 1387-90.
14. Grünewald, K., et al., *Three-dimensional structure of herpes simplex virus from cryo-electron tomography*. Science, 2003. **302**(5649): p. 1396-8.
15. Cyrklaff, M., et al., *Cryo-electron tomography of vaccinia virus*. Proc. Natl. Acad. Sci. U.S.A., 2005. **102**(8): p. 2772-7.
16. Kürner, J., A.S. Frangakis, and W. Baumeister, *Cryo-electron tomography reveals the cytoskeletal structure of Spiroplasma melliferum*. Science, 2005. **307**(5708): p. 436-8.
17. Frangakis, A.S. and R. Hegerl, *Noise reduction in electron tomographic reconstructions using nonlinear anisotropic diffusion*. J. Struct. Biol., 2001. **135**(3): p. 239-50.
18. Benjamin, J., et al., *Three-dimensional structure of HIV-1 virus-like particles by electron cryotomography*. J. Mol. Biol., 2005. **346**(2): p. 577-588.

19. Cannon, G.C., et al., *Microcompartments in prokaryotes: carboxysomes and related polyhedra*. Appl. Environ. Microbiol., 2001. **67**(12): p. 5351-61.
20. Mouche, F., et al., *Automated three-dimensional reconstruction of keyhole limpet hemocyanin type I*. J. Struct. Biol., 2003. **144**(3): p. 301-12.
21. Heymann, J.B., *Bsoft: image and molecular processing in electron microscopy*. J. Struct. Biol., 2001. **133**(2-3): p. 156-69.
22. Frank, J., *Single-particle imaging of macromolecules by cryo-electron microscopy*. Annu. Rev. Biophys. Biomol. Struct., 2002. **31**: p. 303-19.

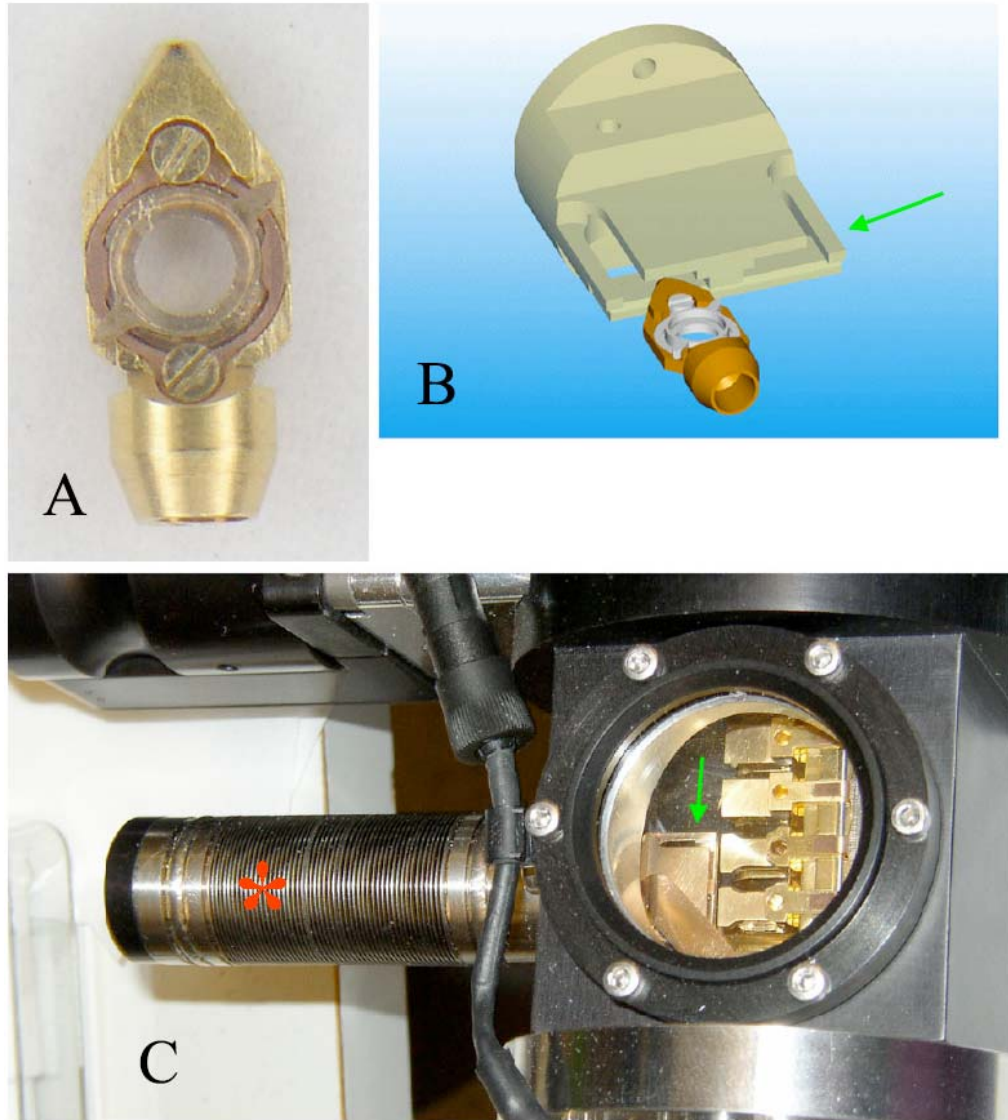
Figures and Table

Figure A-1. Flip-flop rotation stage.

Panel A: Photograph of a flip-flop cartridge. The lower (non-pointed) end houses threads used to mount the cartridge to the end of the specimen rod, which resides permanently in the microscope. The inner cup can be rotated, and has two protrusions seen here at “2” and “8 o’clock.” For scale, the cup circumscribes grids 3 mm across. Panel B: A drawing

of a flip-flop cartridge positioned in front of the rotation tool (courtesy FEI Company and Gatan UK). The rotation tool is like a two-car garage in that it could house the cartridge in either of two positions, here seen as “left” and “right” sides. If the rotation tool were pushed over the cartridge as aligned in the drawing, its front edge would catch the right cup protrusion and cause the cup to rotate 90°. Panel C: a photograph of the part of the multispecimen holder that houses the rotation tool. Through the circular glass window on top, cartridge docking positions 3 (top) through 6 (bottom) are visible on the right, and the front edge of the rotation tool is visible on the left (green arrows in panels B and C point to rotation tool in the same orientation). Pushing the bellowed piston (red asterisk) seen on the left side of the photograph moves the tool over and around cartridge docking positions 5 and 6, rotating any cartridges that may be present into either the flip or flop orientation, depending on their position.

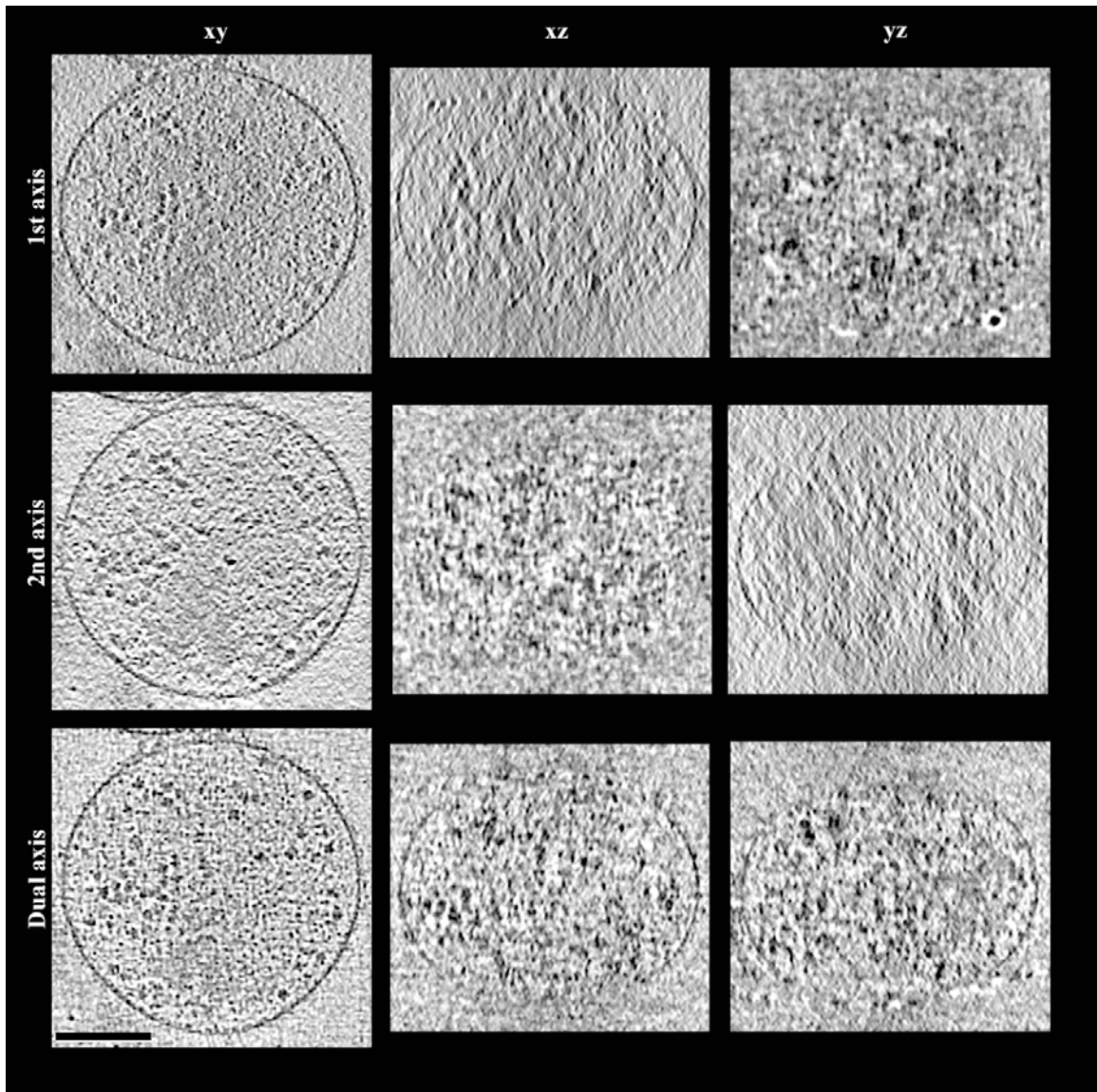


Figure A-2. Single- and dual-axis tomograms of an intact cell.

On the top, middle, and bottom rows are shown single slices of the first single-axis tomogram, the second single-axis tomogram, and the combined dual-axis tomogram, respectively, of an intact *M. florum* cell. The left, middle, and right columns show XY, XZ, and YZ slices, respectively. While individual macromolecular complexes are visible in the XY slices of all three tomograms, only in the dual-axis tomogram are the densities resolved (punctate) in all three directions. The extended but still not complete definition

A-24

of the membrane clearly reveals the improved but still anisotropic point-spread-function.

(Scale bar is 150 nm.)

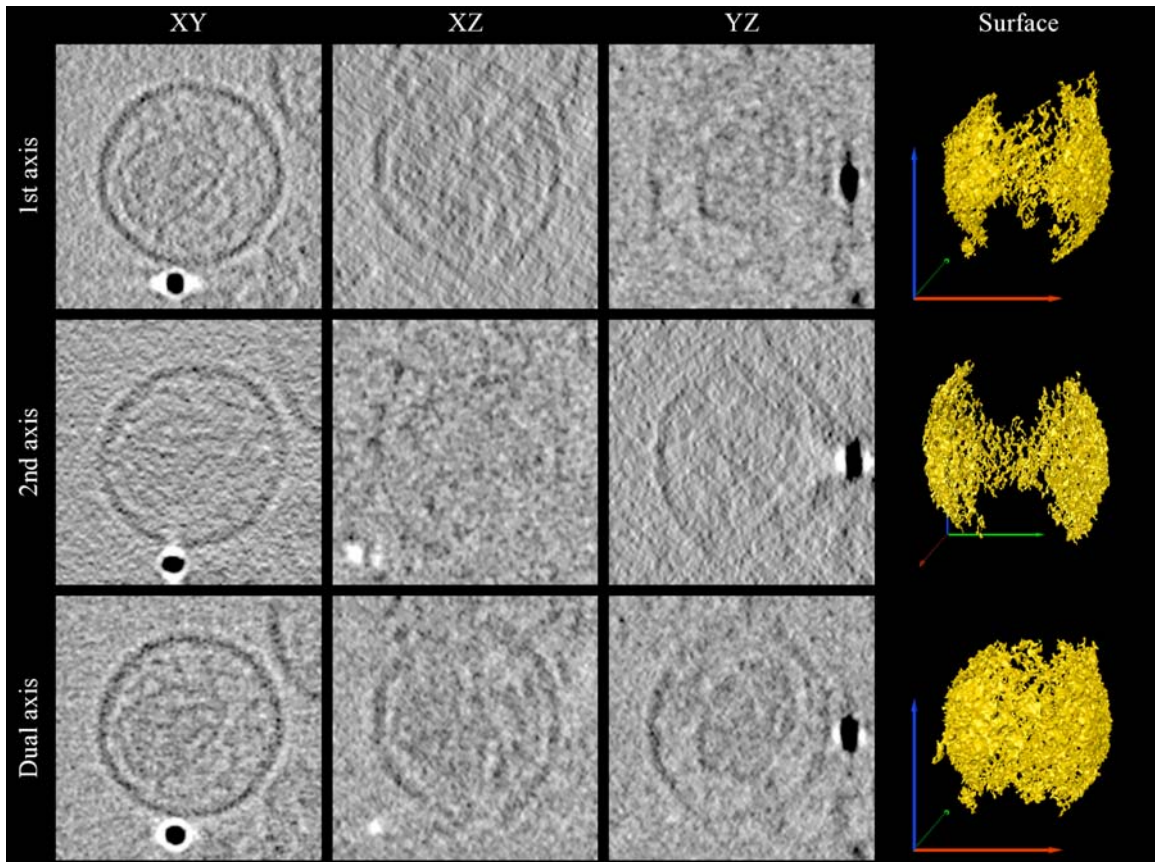


Figure A-3. Single- and dual-axis tomograms of an HIV-1 virus-like particle.

XY, XZ, and YZ slices from the first single-axis tomogram (top), the second single-axis tomogram (middle), and the combined dual-axis tomogram (bottom) of an HIV-1 virus-like particle are shown as in Fig. A-2. The outer bilayer/matrix layer and the capsid are visible. A single gold fiducial also appears at the bottom of the XY slices and on the right side of the YZ slices, which shows well the asymmetry of the point-spread-function in the single-axis tomograms. Dual-axis tilting makes this point-spread-function round in the XY slice, but it is still elongated in the Z direction. Three-dimensional renditions of the continuous envelope density are shown on the far right (note that the view in the second row has been rotated 90° relative to the others to show its missing wedge). These isosurfaces were defined by the “Magic Wand” tool in the Amira software package,

which marks voxels that are both connected to an initial seed voxel and have densities higher than a user-specific value. (For scale, the diameters of the gold fiducial and virus-like particle are 10 and ~ 125 nm, respectively.)

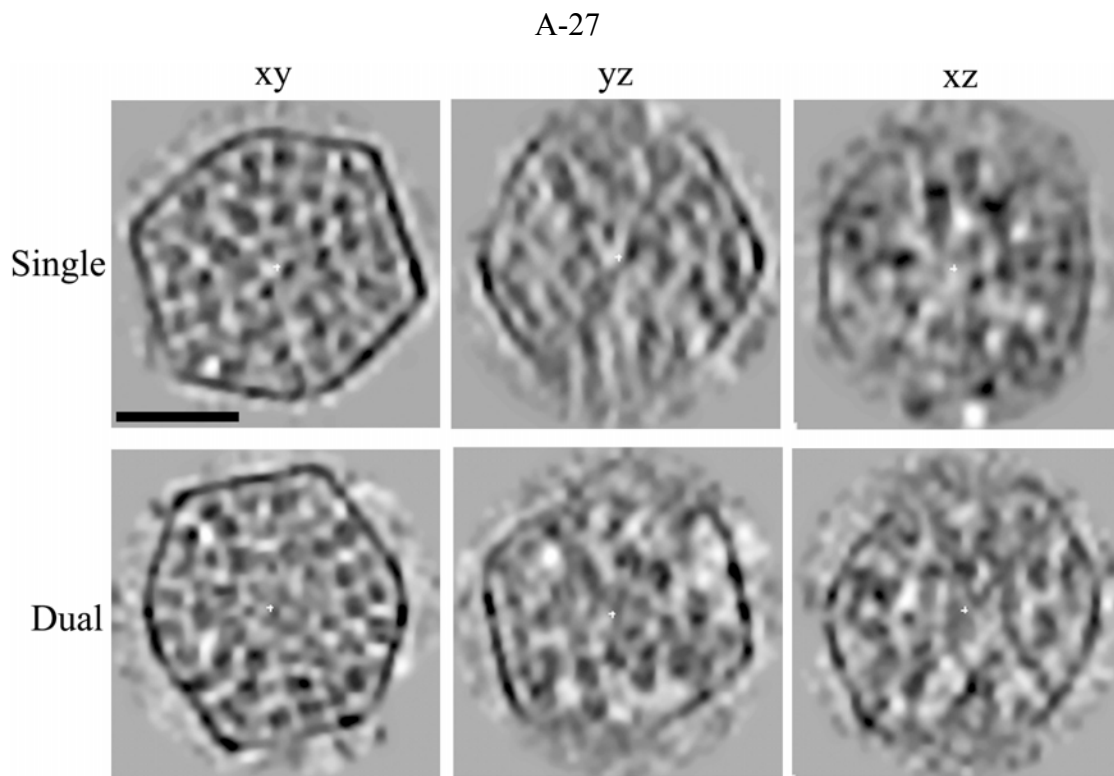


Figure A-4. Single- and dual-axis tomograms of prokaryotic carboxysomes.

XY, YZ, and XZ slices through the tomograms of two different carboxysomes are shown.

The outer protein shell can be seen enclosing many tens of RuBisCO enzymes inside.

Each tomogram used the same total dose, so the improvements in the dual-axis tomogram

are due to data collection geometry rather than any increase in dose. (Scale bar is

50 nm.)

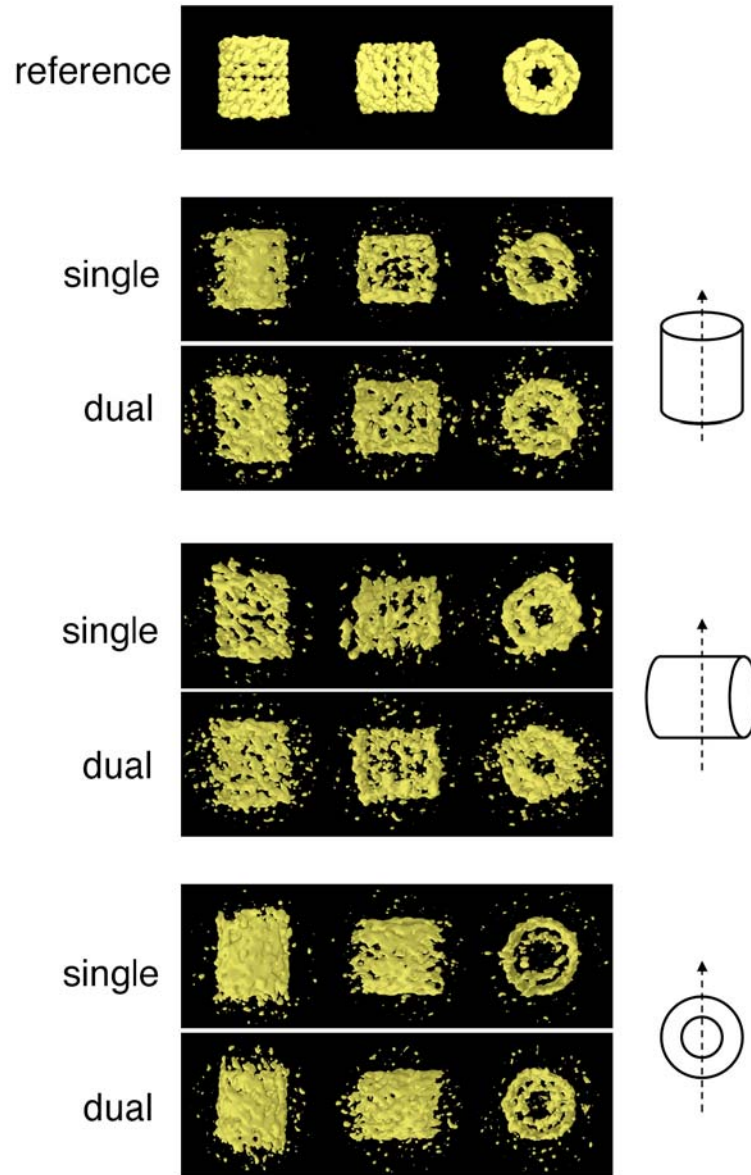


Figure A-5. Single- and dual-axis tomograms of individual protein complexes.

Surface renderings of seven independent reconstructions of the barrel-shaped hemocyanin protein complex are shown. Each row presents one reconstruction, seen from three different points of view. The top row displays the 12 Å “single-particle” reconstruction obtained by averaging hundreds of projection images [20], and is shown for comparison and orientation. The even- and odd-numbered rows show single- and dual-axis tomograms, respectively, generated with the same total dose. The particular

particles shown were chosen to control for and reveal how orientation in the ice, as depicted on the right, influenced the results. In the schematic, the dotted line represents the tilt axis (or the first tilt axis in the case of the dual-tilt tomograms), and the plane of the schematic represents the plane of the grid. Simple isosurfaces are shown, contoured at 2.5 standard deviations above the mean. (For scale, hemocyanin is ~ 35 nm in length.)

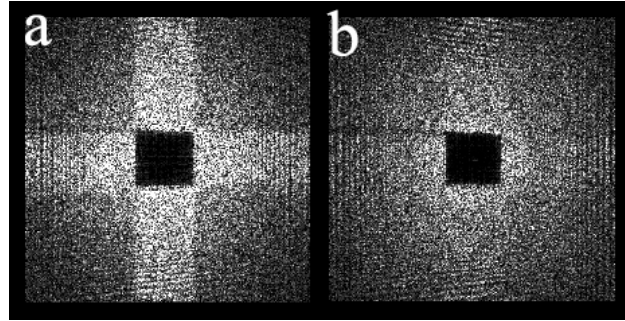


Figure A-6. Missing pyramid and intensity scaling.

Sections from the three-dimensional power spectrum of a reconstructed *M. florum* cell are shown. Both are the fortieth XY section above the central “ $Z = 0$ ” section, so that the missing pyramid is visible as a square in the middle. In (a), the overweighed intensities in the singly-measured regions of reciprocal space appear as a bright cross. The same section is shown in (b) after application of the new intensity scaling function.

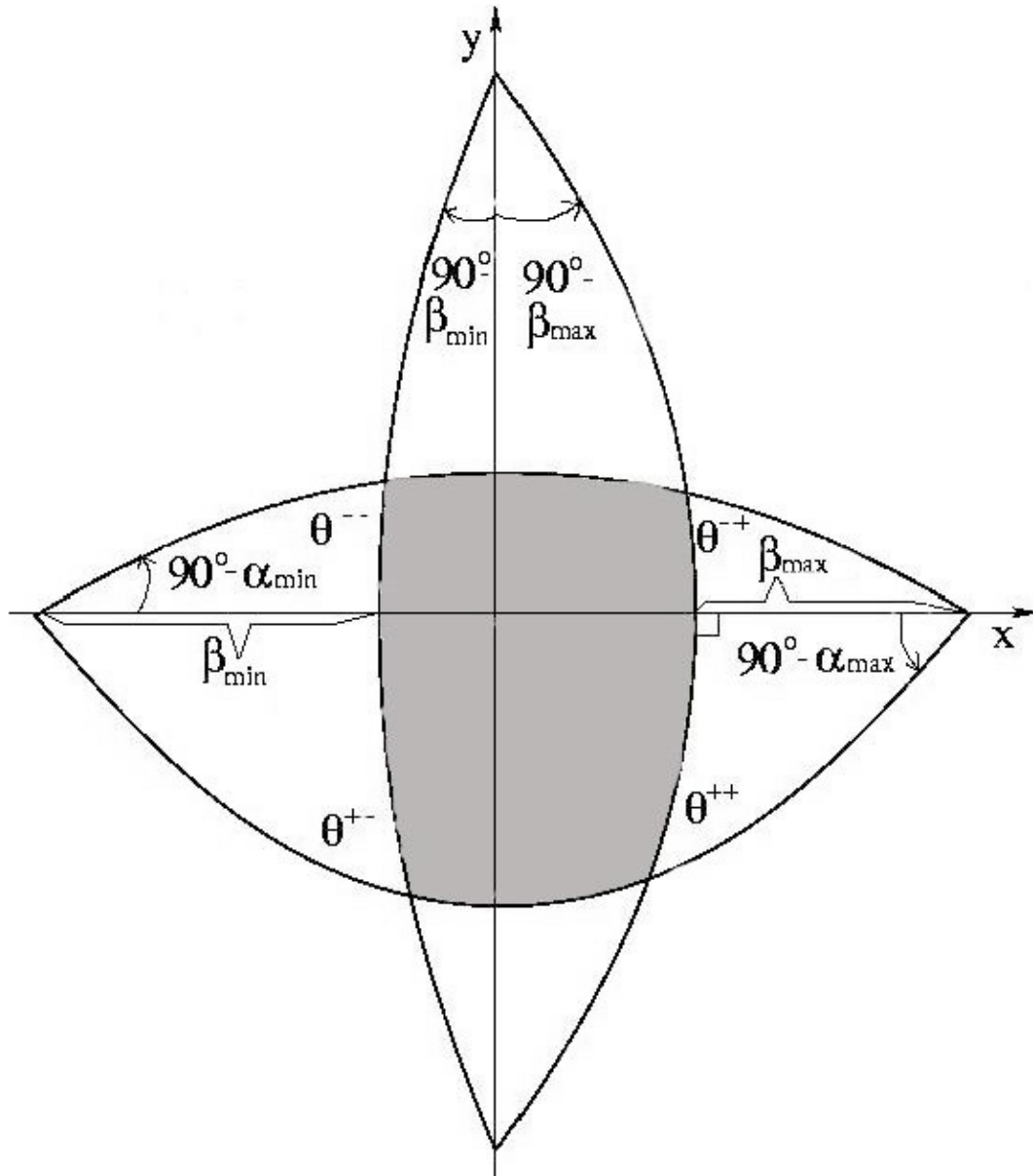


Figure A-7. Diagram used to find the area of the “missing pyramid.”

The four large arcs delineate the angular limits of data collection in the two orthogonal tilt-series (α_{\min} , α_{\max} , β_{\min} , and β_{\max}) on the surface of a sphere in reciprocal space. The area of the missing pyramid is equal to the “angular excess” of the shaded spherical quadrilateral, and is found as described in the text.

Tilt range	Thickness increase at angular extreme	Percent of reciprocal space unmeasured	
		Single-axis data collection	Dual-axis data collection
$\pm 60^\circ$	2.0_	33%	16%
$\pm 67^\circ$	2.6_	26%	10%
$\pm 70^\circ$	2.9_	22%	7.5%
$\pm 81^\circ$	6.4_	10%	1.6%

Table A-1. Percent coverage of reciprocal space in single- and dual-axis tomography.